Activity of Bisphosphonates against *Trypanosoma brucei rhodesiense*

Michael B. Martin,[§] John M. Sanders,[§] Howard Kendrick,[†] Kate de Luca-Fradley,[†] Jared C. Lewis,[§] Joshua S. Grimley,[§] Erin M. Van Brussel,[§] Jeffrey R. Olsen,[§] Gary A. Meints,[§] Agnieszka Burzynska,[‡] Pawel Kafarski,[‡] Simon L. Croft,[†] and Eric Oldfield*[,§,#]

Department of Chemistry, University of Illinois at Urbana-Champaign, 600 South Mathews Avenue, Urbana, Illinois 61801, Department of Infectious and Tropical Diseases, London School of Hygiene and Tropical Medicine, Keppel Street, London WC1E 7HT, U.K., Institute of Organic Chemistry, Biochemistry and Biotechnology, Wroclaw University of Technology, Wroclaw, Poland, and Department of Biophysics, University of Illinois at Urbana-Champaign, 600 South Mathews Avenue, Urbana, Illinois 61801

Received June 20, 2001

We report the results of a comparative molecular field analysis (CoMFA) investigation of the growth inhibition of the bloodstream form of *Trypanosoma brucei rhodesiense* trypomastigotes by bisphosphonates. A quantitative three-dimensional structure−activity relationship CoMFA model for a set of 26 bisphosphonates having a range of activity spanning ∼3 orders of magnitude (minimum IC_{50} = 220 nM; maximum IC_{50} = 102 μM) yielded an R^2 value of 0.87 with a cross-validated R^2 value of 0.79. The predictive utility of this approach was tested for three sets of three compounds: the average pIC_{50} error was 0.23. For the nitrogen-containing bisphosphonates, in general, the activity was aromatic- ≫ aliphatic-containing side chains. The activity of aromatic species lacking an alkyl ring substitution decreased from ortho to meta to para substitution; halogen substitutions also reduced activity. For the aliphatic bisphosphonates, the IC_{50} values decreased nearly monotonically with increasing chain length (down to IC_{50} = 2.0 μM for the *n*-C_{11} alkyl side chain species). We also show, using a "rescue" experiment, that the molecular target of the nitrogen-containing bisphosphonate, risedronate, in *T. b. rhodesiense* is the enzyme farnesyl pyrophosphate synthase. In addition, we report the LD_{50} values of bisphosphonates in a mammalian cell general toxicity screen and present a comparison between the therapeutic indices and the IC_{50} values in the *T. b. rhodesiense* growth inhibition assay. Several bisphosphonates were found to have large therapeutic indices (≳200:1) as well as low IC_{50} values, suggesting their further investigation as antiparasitic agents against *T. b. rhodesiense*.

Introduction

The parasitic protozoa *Trypanosoma brucei gambiense* and *T. b. rhodesiense* are the causative agents of human African trypanosomiasis (sleeping sickness), responsible for over 500 000 disease cases annually.[1] The most widely used treatment for second-stage central nervous system (CNS) infection by these *T. brucei* sspp. is melarsoprol, an arsenic-based compound discovered more than 50 years ago.[2,3] However, melarsoprol must be administered intravenously, and the caustic nature of the vehicle damages veins. Consequently, 5% of those treated die from the acute encephalopathy resulting from the treatment.[4] In addition, there is an increasing occurrence of *T. b. gambiense* resistance to melarsoprol treatment.[5]

In the search to identify new drugs for the treatment of parasitic protozoan diseases, some promising new developments have recently emerged. For example, Vaniqa (eflornithine), an ornithine decarboxylase inhibitor now used as a cosmetic agent, has been shown to have strong activity against *T. b. gambiense*,[6] the causative agent of West African sleeping sickness, and miltefosine (developed as an anticancer agent, ref 7) has been shown to have strong activity against *Leishmania donovani*,[8] the causative agent of visceral leishmaniasis. More recently, bisphosphonates, a class of compounds that are currently used to treat bone resorption diseases,[9] have also been identified as potent antiparasitic agents.[10−15] Bisphosphonates, such as pamidronate (Novartis' Aredia), alendronate (Merck's Fosamax), and risedronate (Procter and Gamble's Actonel), are hydrolytically stable pyrophosphate analogues containing a P−C−P backbone and act by inhibiting enzymes of the mevalonate or isoprenoid biosynthetic pathway. Many bisphosphonates are known to inhibit farnesyl pyrophosphate synthase (FPPS),[16−21] and in doing so, they inhibit the formation of farnesyl pyrophosphate, a compound used in protein prenylation and in the production of dolichols, ubiquinones, and sterols. In early work, bisphosphonates were also found to inhibit the growth of the protozoan parasite *Entamoeba histolytica*,[22] as well as to be strong inhibitors of *Dictyostelium discoideum* growth,[23] and it was later shown that the potent bone antiresorptive bisphosphonate drug risedronate inhibits FPPS in *D. discoideum*.[21] In our research, we recently reported that risedronate and other bisphosphonates have activity against the in vitro proliferation of *Trypanosoma cruzi*, *Trypanosoma brucei*

* To whom correspondence should be addressed. Telephone: 217-333-3374. Fax: 217-244-0997. E-mail: eo@chad.scs.uiuc.edu.
[§] Department of Chemistry, University of Illinois at Urbana-Champaign.
[†] London School of Hygiene and Tropical Medicine.
[‡] Wroclaw University of Technology.
[#] Department of Biophysics, University of Illinois at Urbana-Champaign.

10.1021/jm0102809 CCC: $22.00
Published on Web 06/05/2002

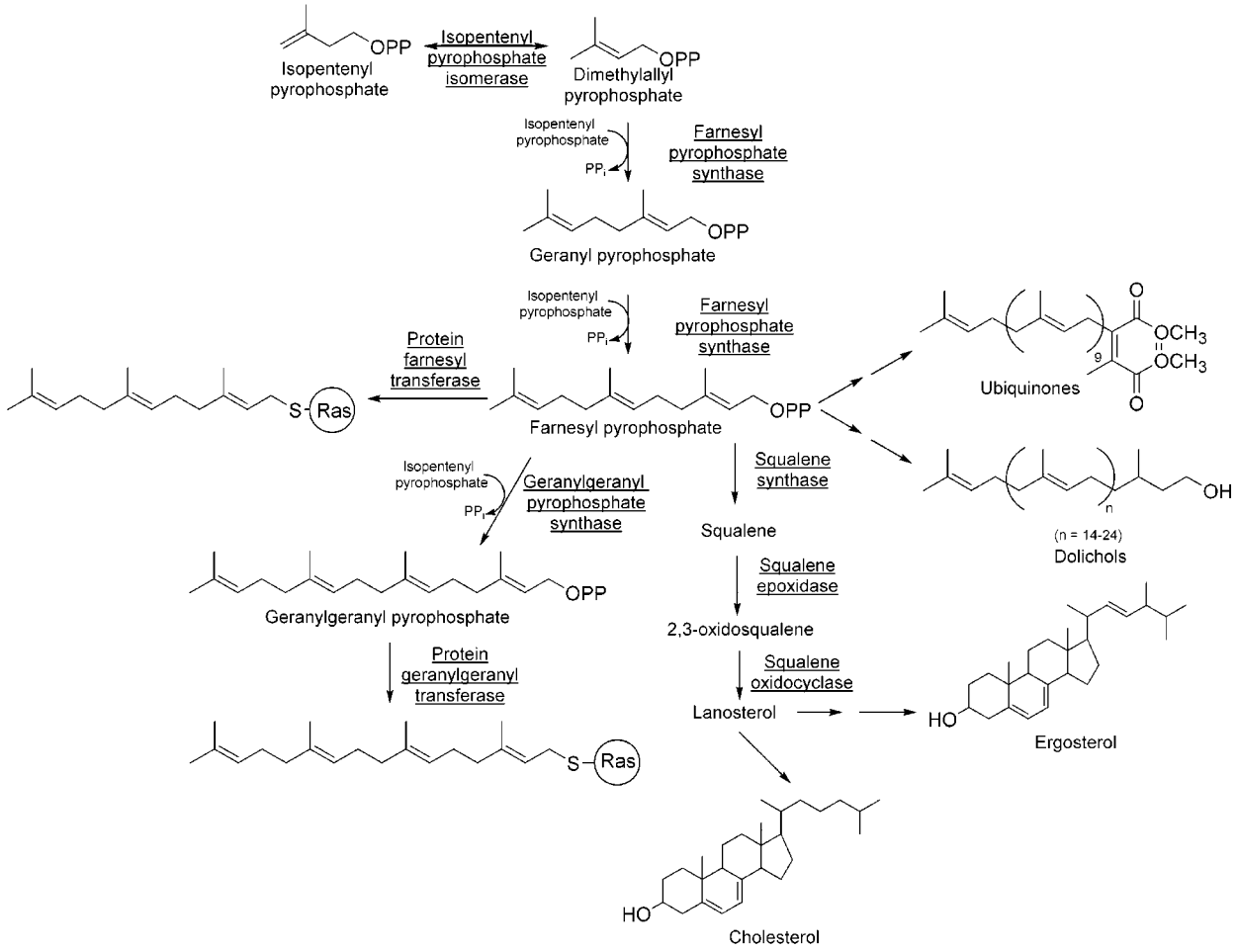

Figure 1. The mevalonate/isoprene pathway showing the biosynthesis of isoprenoids and sterols. The names of the enzymes that catalyze the reactions are underlined. The formation of FPP is an important branch point in this pathway, leading to protein prenylation and the formation of dolichol and sterols, such as ergosterol.

rhodesiense, *Leishmania donovani*, *Toxoplasma gondii*, and *Plasmodium falciparum*.[11,12] Moreover, in the case of *T. cruzi*[11], *L. donovani*,[14] *L. mexicana*,[15] and *Cryptosporidium parvum*,[13] promising results have been found in animal models, including parasitological cures with two *Leishmania* species.[14,15]

Because some bisphosphonates are already FDA-approved for use in humans and possess significant antiparasitic activity, they represent an interesting class of chemotherapeutic agents to try to develop further, and here, we report initial quantitative structure−activity relationship (QSAR) results for bisphosphonate growth inhibition of *T. b. rhodesiense*. We also show that the molecular target of the bisphosphonate risedronate in *T. b. rhodesiense* is FPPS. In addition, we report the toxicological effects of a series of bisphosphonates on growth of a human nasopharyngeal carcinoma (KB strain) cell line, in an effort to identify chemical species having both large therapeutic indices and small IC_{50} values for parasite growth inhibition.

Results and Discussion

The Risedronate Target in *T. b. rhodesiense*. On the basis of published results with *Dictyostelium discoideum* growth inhibition,[21,23] as well as extensive work in plants and animals,[16−20] it appeared that the most likely site of action of the potent nitrogen-containing bisphosphonates, such as risedronate, in parasitic protozoa was the enzyme farnesyl pyrophosphate synthase (FPPS). This enzyme catalyses the condensation of dimethylallyl pyrophosphate (DMAPP) with isopentenyl pyrophosphate (IPP, Figure 1) to form geranyl pyrophosphate, which then condenses with a second molecule of IPP to form farnesyl pyrophosphate (FPP). FPP can then be used to prenylate proteins or to form geranylgeranyl pyrophosphate (GGPP), dolichols, ubiquinones, and sterols (Figure 1). We also recently proposed, on the basis of molecular modeling and quantum chemical calculations, that bisphosphonates act as (aza)carbocation inhibitors of FPPS because they can mimic the reactive intermediates that are thought to occur in FPP synthesis.[24] If this view is correct, then it should be possible to reverse bisphosphonate inhibition with the end product, FPP, and indeed in osteoclasts, bisphosphonate inhibition has been reversed by addition of FPP (and in some cases farnesol, GGPP, or geranylgeraniol).[17,25]

To determine whether FPPS is the target for at least the more potent nitrogen-containing bisphosphonates in *T. b. rhodesiense*, we carried out a series of in vitro "rescue" experiments, Table 1, in which we investigated the reversal of risedronate-induced growth inhibition of *T. b. rhodesiense* bloodstream-form trypomastigotes by GPP, FPP, or farnesol. As can be seen in Table 1,

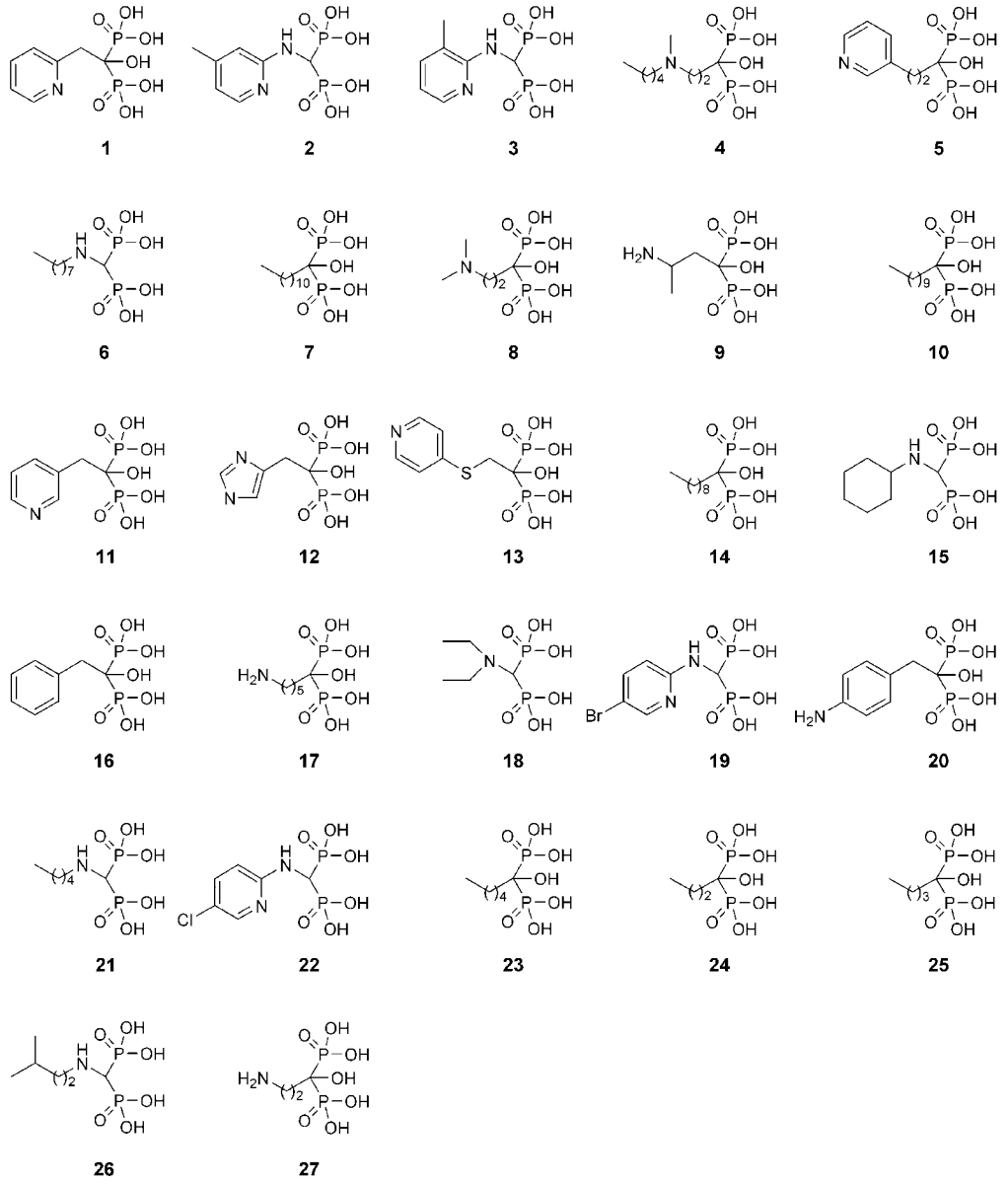

Figure 2. Structures of bisphosphonates investigated, ordered by decreasing activity.

Table 1. In Vitro Rescue of Risedronate Growth Inhibition (Reported as Percent Inhibition) of *T. brucei rhodesiense*

drug combination	risedronate concentration (μM)						IC_{50} (μM)
	83.54	27.85	9.27	3.09	1.03	0.33	
risedronate	100	100	86.49	23.49	19.30	0	4.12
risedronate + GPP[a]	100	100	83.70	44.59	0		3.71
risedronate + FPP[b]	64.24	25.40	0				66.80
risedronate + farnesol[c]	0						>83.54

[a] Geranylpyrophosphate (GPP), 12.5 μg/mL. [b] Farnesylpyrophosphate (FPP), 12.5 μg/mL. [c] Farnesol, 12.5 μg/mL.

risedronate (**11**, Figure 2) substantially inhibits the in vitro proliferation of bloodstream-form *T. b. rhodesiense* trypomastigotes. However, this growth inhibition is dramatically reduced when an exogenous source of FPP is provided, resulting in more than a 16-fold increase in the apparent IC_{50} value, Table 1. Furthermore, the addition of exogenous farnesol completely rescued cells from risedronate inhibition. The more effective rescue by farnesol over farnesyl pyrophosphate may be attributable to the greater uptake of the alcohol, and similar results have been seen in some bone resorption studies.[25] Geranyl pyrophosphate (GPP), the upstream substrate just prior to FPP in the mevalonate pathway (Figure 1), provided no rescue from risedronate inhibition.

These results are all consistent with the hypothesis that farnesyl pyrophosphate synthase is a principal target of the nitrogen-containing bisphosphonates in *T. b. rhodesiense*, consistent with previous findings in plants,[16] in animals,[17−20] and in *D. discoideum*.[21] These results are also consistent with other results that we have found in protozoan systems. Specifically, we recently showed that risedronate inhibits *Trypanosoma cruzi* and *Leishmania major* sterol biosynthesis at a presqualene level[12] and that risedronate and other bisphosphonates are potent *T. cruzi* FPPS inhibitors.[26] This is consistent with the rescue results presented in Table 1. The results presented in Table 1 also imply that the molecular target of the nitrogen-containing bisphos-

Table 2. Experimental (IC_{50} and pIC_{50}) and CoMFA Predicted (pIC_{50}) Values for Bisphosphonates against *T. Brucei* Trypomastigotes and Statistical Results of 3D-QSAR CoMFA Models

	experimental activity		predicted pIC_{50}[b]			
compound[a]	IC_{50} (μM)	pIC_{50}	training set	3-compound test sets		
1 (*ortho*-risedronate)	0.22	6.66	5.93 (6.68)	5.98 (6.59)	6.22 (6.65)	5.94 (6.69)
2	0.61	6.21	6.31 (5.80)	6.37 (5.74)	6.29 (5.79)	6.31 (5.80)
3	0.70	6.15	6.30 (5.88)	**6.37 (5.81)**	6.30 (5.87)	6.31 (5.88)
4 (ibandronate)	0.96	6.02	6.37 (5.84)	6.42 (5.83)	**6.12 (5.80)**	6.37 (5.86)
5 (homorisedronate)	1.7	5.77	5.42 (6.21)	5.44 (6.17)	5.57 (6.21)	5.43 (6.26)
6	1.7	5.77	5.49 (5.51)	5.51 (5.51)	5.57 (5.49)	5.50 (5.52)
7	2.0	5.70	5.29 (5.35)	5.29 (5.34)	5.27 (5.32)	5.29 (5.32)
8 (olpadronate)	5.4	5.27	5.34 (5.18)	**5.36 (5.16)**	5.31 (5.20)	5.34 (5.23)
9	7.8	5.11	4.96 (4.57)	4.96 (4.57)	4.94 (4.61)	4.97 (4.62)
10	8.0	5.10	5.29 (5.35)	5.29 (5.34)	5.27 (5.32)	5.29 (5.32)
11 (risedronate)	8.6	5.07	5.00 (5.05)	5.03 (5.03)	**5.85 (5.04)**	5.02 (5.11)
12	8.6	5.07	5.17 (5.24)	5.20 (5.22)	5.42 (5.26)	**5.18 (5.31)**
13	19.8	4.70	4.62 (4.50)	4.60 (4.51)	4.62 (4.53)	4.62 (4.53)
14	20.5	4.69	5.29 (5.35)	5.29 (5.34)	5.27 (5.32)	5.29 (5.32)
15	20.9	4.68	4.44 (4.55)	4.41 (4.54)	4.65 (4.60)	4.44 (4.60)
16	21.3	4.67	4.86 (4.17)	4.88 (4.16)	4.15 (4.24)	4.87 (4.19)
17 (neridronate)	31.7	4.50	4.62 (4.48)	4.61 (4.51)	4.51 (4.46)	4.63 (4.50)
18	34.4	4.46	4.44 (4.47)	4.41 (4.46)	4.66 (4.53)	**4.44 (4.52)**
19	39.5	4.40	4.30 (4.60)	4.30 (4.57)	4.22 (4.60)	4.32 (4.60)
20	40.0	4.40	4.68 (4.35)	4.69 (4.35)	4.60 (4.31)	4.70 (4.33)
21	50.6	4.30	4.40 (4.50)	4.37 (4.49)	4.62 (4.56)	4.41 (4.55)
22	53.3	4.27	4.30 (4.58)	4.29 (4.54)	4.20 (4.57)	**4.31 (4.58)**
23	62.4	4.20	4.00 (4.16)	3.94 (4.15)	4.15 (4.23)	4.01 (4.18)
24	92.0	4.04	4.00 (4.17)	**3.94 (4.15)**	4.15 (4.23)	4.01 (4.18)
25	99.8	4.00	4.00 (4.16)	3.94 (4.15)	4.15 (4.23)	4.01 (4.18)
26	102	3.99	4.39 (4.51)	4.36 (4.50)	**4.61 (4.57)**	4.40 (4.56)
27 (pamidronate)	$\gg$100	<4.00				
R^2[c]			0.87 (0.84)	0.85 (0.83)	0.88 (0.85)	0.86 (0.84)
F_{test}[d]			34.80 (28.50)	26.36 (21.46)	31.82 (24.67)	28.42 (24.05)
R_{cv}^2[e]			0.79 (0.77)	0.73 (0.73)	0.79 (0.75)	0.77 (0.75)
R_{bs}^2[f]			0.87 (0.85)	0.86 (0.83)	0.88 (0.85)	0.86 (0.84)
N[g]			5	5	5	5
N[h]			26	23	23	23

[a] See Figure 2. **1**−**3**, **5**, **7**−**13**, **16**, **17**, **20**, **23**−**25**, and **27** cited from ref 12. [b] Bold values represent predicted activities of compounds that were not included in the training set. [c] Correlation coefficient. [d] Ratio of R^2 explained to unexplained $= R^2/(1 - R^2)$. [e] Cross-validated correlation coefficient after leave-one-out procedure. [f] Average squared correlation coefficient calculated during the validation procedure. [g] Optimal number of principal components. [h] Number of compounds.

phonate risedronate (**11**) in *T. b. rhodesiense* is FPPS and not IPP isomerase, because GPP does not afford any significant rescue from growth inhibition. This observation makes it unlikely that IPP isomerase is the target for **11**, because it is IPP isomerase that produces DMAPP from IPP produced by the mevalonate pathway, Figure 1, and therefore, GPP should rescue from an IPP isomerase inhibitor. However, both FPP and farnesol afford a rescue, Table 1, a pattern seen also by Benford et al. in their bone resorption work.[25] Both farnesol and farnesyl phosphate kinases are known in rats and are presumably also present in *T. brucei*.

Of course, it is not possible to be certain that all of the bisphosphonates investigated bind to the same target in the same way. Nevertheless, because many of the compounds investigated are known FPPS inhibitors, it appeared that a more detailed investigation between structure (Figure 2) and activity (Table 2) would be worthwhile, testing the idea that it might be feasible to extract interesting and predictively useful information on activity by using 3D QSAR/CoMFA methods to analyze the growth inhibition results.

QSAR/CoMFA Investigations. In previous work, we reported the inhibition by bisphosphonates of *T. b. rhodesiense* trypomastigote growth,[12] and we have now used this information, together with additional results, to develop a QSAR/CoMFA model for bisphosphonate growth inhibition. As a starting point, we investigated all 17 bisphosphonates previously found to have IC_{50} values <200 μM,[12] together with new data for nine more compounds (Figure 2), plus pamidronate. This library consists of both nitrogen-containing and non-nitrogen-containing species (Figure 2). Bisphosphonate structures were generated and geometry-optimized by using a three-step protocol consisting of steepest-decent, conjugate-gradient, and Newton−Raphson minimizations, with no constraints on the internal geometries of the molecules, using the Minimizer function of the OFF Methods module in Cerius^2 4.6.[27] Each molecule was aligned to the lowest energy conformation of the most active compound, **1**, by performing a rms fitting of the P−C−P backbone atoms of each conformer to those of the template using the Shape Reference Alignment function of the QSAR module of Cerius^2 4.6. The alignments of each structure, obtained through pairwise superpositioning using the maximum common subgroup method, placed all structures in the study table in the same reference frame as the shape reference compound, as shown in Figure 3. The structure of the lowest energy conformer of **1** (*ortho*-risedronate) is remarkably similar to one of the crystallographic structures of risedronate (**11**),[28] as shown in Figure 4A, giving some confidence to this approach. In addition, the alignment of essentially all of the bisphosphonates could be readily docked into the putative (DMAPP/GPP) substrate binding site of (an avian) FPPS, Figure 4B, with the longer chain bisphosphonates readily mapping onto the GPP substrate, again supporting the alignment. We also

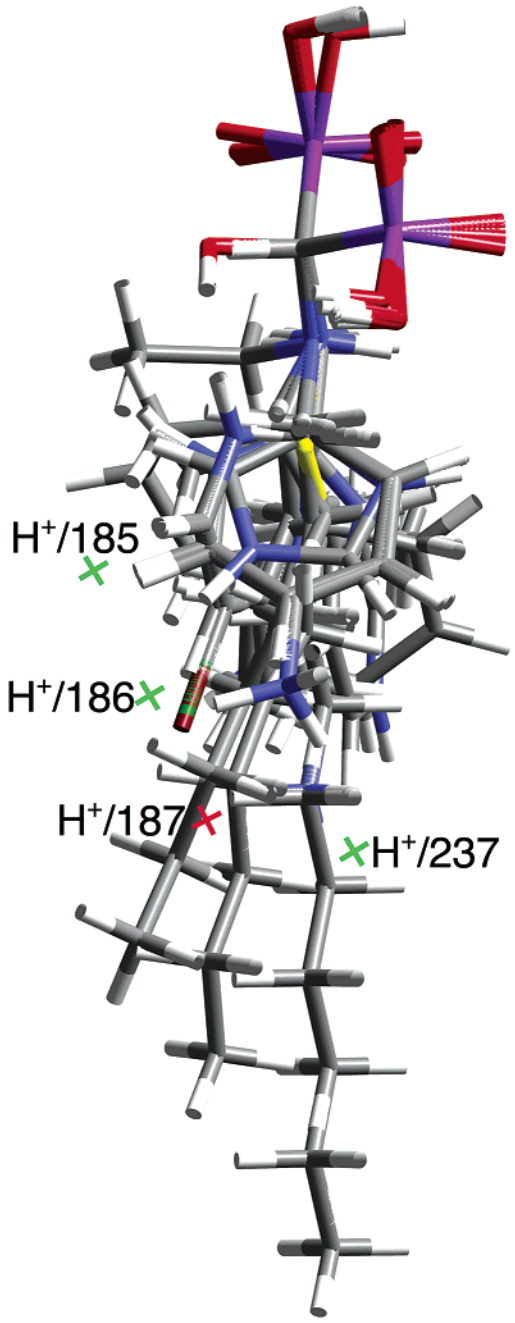

Figure 3. 3D-QSAR/CoMFA structure alignment; superposition of 26 compounds.

carried out a second set of calculations, this time starting with the backbone conformation found in a crystal structure of incadronate.[29] Only the MM/risedronate alignment, which gave the best QSAR statistics (Table 2), is shown in Figure 4A, and this yielded the overall alignment shown in Figure 4B. Predicted results for both alignments are given in Table 2. In all cases, we used bisphosphonates containing protonated nitrogens and monoprotonated phosphonate groups $[P(O)_2(OH)]^{-1}$. This pattern of protonation is observed in many bisphosphonates and is also observed in the X-ray crystallographic structure of **5** (sodium homorisedronate tetrahydrate), from which we obtained the structure shown in Figure 5.

CoMFA 3D-QSAR methodology was then applied to the in vitro growth inhibition data to help identify the structural features required for activity against *T. b. rhodesiense* replication. We applied a regression analysis to the data, leading to eq 1:

$$pIC_{50} = 4.60 - 0.06"H^+/187" + 0.02"H^+/237" + 0.05"H^+/186" + 0.01"H^+/185" \quad (1)$$

where the H^+ descriptors define the corresponding interaction energies between a proton probe and the molecule at the specified (numbered) grid points (see Figure 3 for their locations). The 3D-QSAR/CoMFA equation was calculated using a genetic function approximation (GFA) algorithm.[30] The genetic function approximation involves starting with an initial population of random equations, which are then allowed to evolve by application of crossover operations such that terms from models with the best fit will most likely occur in the "offspring models". Best-fit models are retained, while poor-fit models are replaced with subsequent generations. The optimal number of components in the final GFA model was determined by cross-validated R^2 values as obtained from the leave-one-out cross-validation technique,[31] standard error prediction values, and also by F-test values. The CoMFA model containing the five components shown above afforded a correlation coefficient of 0.87 and a cross-validation R_{cv}^2 of 0.79. These statistical parameters are given in Table 2, along with experimental and predicted pIC_{50} ($-\log IC_{50}$ (M)) values. The training set results for the 26 compounds are shown graphically in Figure 6A, and a confidence limit of 95% was established using the data randomization procedure in Cerius[2] 4.6. The second alignment (based on an alternative bisphosphonate side chain conformation) gave less good results in all cases, shown in parentheses in Table 2.

We next carried out a series of calculations to test whether eq 1 had predictive value. To do this, we deleted three points at random from the training set, then recomputed the QSAR/CoMFA equations, thereby predicting the three-excluded pIC_{50} values. In all cases, the CoMFA test set equations so obtained contained the same grid point descriptors as the training set equation. This indicates that the QSAR (eq 1) was well determined and that it was not overly sensitive to the training set. The results for three such sets of calculations (nine points for each alignment) are given in Table 2, in which the predicted values are shown as bold entries. Figure 6B shows the results of the nine predictions from the alignment shown in Figure 3 graphically, together with the respective training set results. The average pIC_{50} error for the nine predicted values from the three sets of calculations was 0.23, corresponding to about a factor of 2 uncertainty in the IC_{50} predictions.

The results shown in Table 2 and in Figure 6 are of interest because they suggest that it is possible to predict, with reasonable accuracy, the IC_{50} values for *T. b. rhodesiense* growth inhibition by bisphosphonates, as found also with *D. discoideum* growth inhibition,[32] bone resorption,[32] and geranylgeranyl pyrophosphate synthase inhibition,[33] an ability which may be of use in future drug design work, even though the inhibition data was obtained on intact cells, not on a purified enzyme. In addition, there are clearly several interesting structure−activity relationships evident in the IC_{50} data, which we describe below.

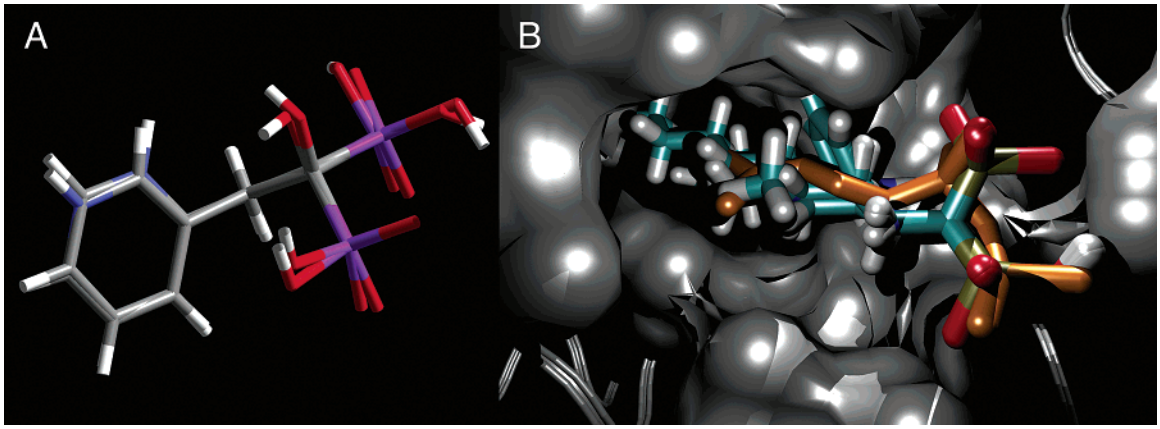

Figure 4. Alignment graphic: (A) molecular mechanics structure of the most active species (**1**) superimposed on a crystal structure of risedronate (**11**); (B) superposition of **1**, **3**, **4**, and **7** on GPP (orange colored) in avian FPPS (PDB accession number 1UBW). Surface drawn for residues surrounding GPP with a 1.4 Å radius probe, using the VMD program.[46]

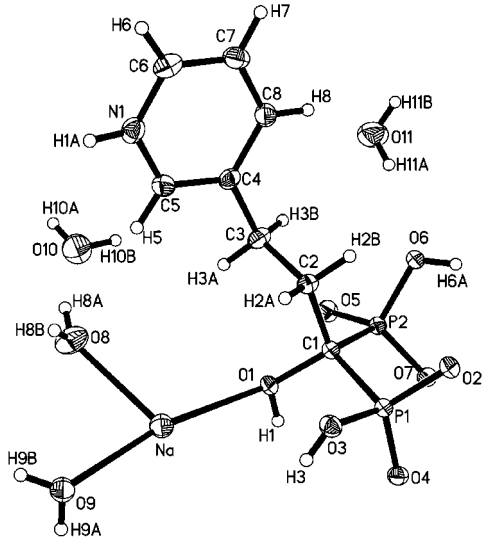

Figure 5. Single-crystal X-ray structure of **5** showing protonation sites.

Activities of Individual Compounds. We next consider the activities of the compounds investigated on an individual basis. Here, it is instructive to refer to Figure 2, in which we show the structures of the molecules studied in order of increasing IC_{50} values (**1**−**26**, plus pamidronate, **27**). We first consider the most and least active compounds: **1** (*ortho*-risedronate, IC_{50} = 220 nM) and **27** (pamidronate, $IC_{50} \gg 100\ \mu M$). Both molecules are nitrogen-containing hydroxy-bisphosphonates with the nitrogen atom separated by two carbons from the bisphosphonate carbon backbone (a γ-nitrogen). However, as can be seen from Table 2, the presence of a γ-N is not a sufficient requirement for high activity. The additional requirement is that the nitrogen be contained in an aromatic ring, which can be expected to provide enhanced hydrophobicity and some charge delocalization, both of which may contribute to binding to the hydrophobic FPPS active site. The charge delocalization may either mimic the charge delocalization expected in the putative G^+PP^- allylic ion pair or, alternatively, mimic the GPP/FPP carbocations prior to deprotonation.

The next most active compounds, **2** and **3** (IC_{50} = 610 and 700 nM, respectively), again contain the γ-nitrogen and aromatic side chain features noted above, but vary

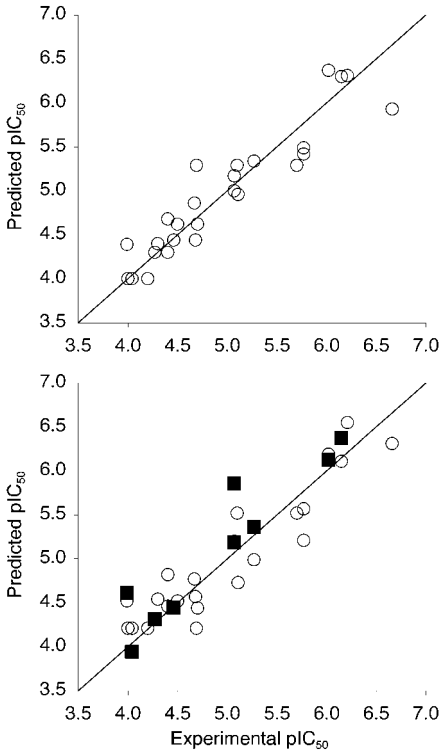

Figure 6. Plot of experimental pIC_{50} versus predicted pIC_{50} values for the 3D-QSAR/CoMFA model of bisphosphonates inhibiting bloodstream-form *Trypanosoma brucei* trypomastigote growth: (A) 26 compound training set; (B) results of the three compound prediction studies for (○) training set and (■) test set.

from **1** in several ways. Most notably, **2** and **3** contain aminomethylene side chains instead of the methylene side chain found in **1**, and both lack the backbone OH substitutions common to the bone resorption drugs, such as pamidronate, alendronate, and risedronate. In addition, both **2** and **3** contain methyl-substituted rings. At present, we cannot be sure as to the reasons for the higher activity of **1** as compared with **2** and **3**, but the aminomethylene side chains of **2** and **3** may contribute to a large energy barrier to χ_2 rotation of the aromatic (quinonoid) ring conformation.[33] Indeed, the X-ray structure of **3**[33] shows a planar α-nitrogen and bond length alternation in the ring, indicating a quinonoid or amidinium-like structure.[33] It thus seems possible

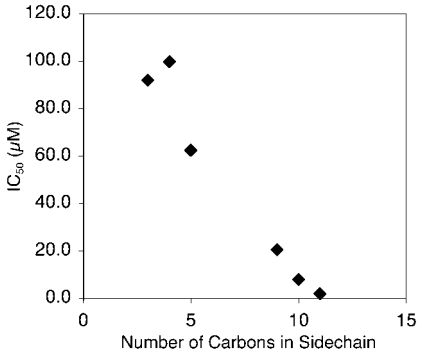

Figure 7. Graph showing apparent correlation between IC_{50} and carbon chain length for the six *n*-alkyl bisphosphonates.

that this could result in slightly different (less favorable) binding geometries for **2** and **3**.

The effect of the arylmethyl substitutions found in **2** and **3** (which are structural isomers) also deserves some comment. These methylations can be expected to increase the hydrophobicity of the side chain, and in many cases, increases in hydrophobicity can increase drug activity. This effect is clearly illustrated in Figure 7, which shows, for the *n*-alkyl bisphosphonates, a near-monotonic decrease in IC_{50} with increasing chain length. This effect could also help explain the high activity of **4** (ibandronate, $IC_{50} = 1.0\ \mu M$) in comparison with **27** (pamidronate, $IC_{50} \gg 100\ \mu M$), because ibandronate contains an *N*-methyl-*N*-pentyl substitution at the γ-N position, and these alkyl substitutuents can interact favorably with the hydrophobic binding pocket. However, in the case of a human recombinant FPP synthase enzyme, and in bone resorption, Dunford et al. found that addition of a single methyl group *ortho* to the side chain of the bisphosphonate NE11808 caused almost a factor of 100 *decrease* in activity, presumably due to a bad steric contact in the FPPS synthase active site, and it is possible that a similar effect may be operative with **2** and **3**. Compound **5**, homorisedronate, has a somewhat higher IC_{50} (1.7 μM), but like NE11808, which also has an elongated side chain,[20] still has considerable activity.

The next series of compounds, **6**−**10**, all have aliphatic side chains and activities in the range of 1.7−8.0 μM. Compound **8** is the known, potent FPP synthase inhibitor olpadronate, the *N*,*N*-dimethyl analogue of pamidronate (**27**, which shows very poor inhibitory activity in this assay) and **6**, **7**, **9**, and **10** have also recently been found to be inhibitors of the FPP synthase of another trypanosomatid, *L. major* (D. Gonzalez-Pacanowska et al., unpublished results) with enzyme inhibition IC_{50} values in the 1−8 μM range. The results for **6**−**10** suggest the importance of hydrophobic interactions for binding, and as noted above, the IC_{50} values for the *n*-alkyl bisphosphonates decrease in an almost monotonic fashion with increasing alkyl chain length (Figure 7). However, incorporation of a side chain nitrogen can, in effect, substitute for the presence of this hydrophobic stabilization, although maximal activity is obtained with both a long alkyl group and a side chain nitrogen, as with ibandronate. The activities of compounds **8** and **9** are not surprising (5.4 and 7.8 μM, respectively) because both contain the γ-N important for maximal activity, but their activity is much less than **4** (ibandronate), which has a longer alkyl chain.

Compounds **11**, **12**, and **13** all have nitrogen-containing aryl side chains and are expected to be active. Compound **11** is the well-known bone resorption inhibitor risedronate and is sold as the drug Actonel. Risedronate has a δ-N in an aromatic ring, while **12**, an isomer of zoledronate, also has an $IC_{50} = 8.6\ \mu M$ and possesses both a γ-N and a δ-N. Both species can be protonated to mimic a carbocation reactive intermediate and have similar charge distributions, as discussed below. On the other hand, **13** (2-(4-pyridylthio)-1-hydroxyethane-1,1-bisphosphonate, $IC_{50} = 19.8\ \mu M$), while it also contains an aromatic side chain containing a nitrogen, has the nitrogen at the ζ position, and this appears to be too far away from the phosphonate backbone to mimic a carbocation reactive intermediate. Indeed there are no known potent FPP synthase inhibitors having this ζ substitution pattern.

Compounds **14**−**20** all have mediocre activity ($IC_{50} = 20.5-40\ \mu M$) because they lack at least one feature needed for maximal activity. Compound **14** lacks a nitrogen; **15** lacks an aromatic ring; **16** lacks a nitrogen; **17** has the side chain nitrogen at a ζ position; **18** lacks a long alkyl group, **19** contains an appropriately positioned aromatic N but the basicity of this N can be expected to be affected by the Br substitution (which may also contribute to a steric repulsion), and **20** again has a ζ nitrogen (as with **13**), which does not confer high activity. Although not promising for chemotherapeutic applications, one SAR of interest that emerges from these results is that, from comparison of **6** and **14**, each having nine heavy atoms in their side chains, the α-N contributes ~100-fold to activity. For the remainder of the compounds (**21**−**27**), there is a general pattern of decreasing activity with decreasing chain length with the aliphatic compounds (Figure 7), but this group of compounds overall are ~100-fold less active than the aromatic N-containing bisphosphonates (**1**−**3**), making them unsuitable for further development.

Quantum Chemical Charge Distributions. We next consider the extent to which the charge on the pyridinium nitrogens in the more active compounds is distributed, because this can be expected to be of use in further developing these compounds for chemotherapeutic applications. In previous work, we and a number of other groups have investigated the electrostatic potential surfaces, $\Phi(\mathbf{r})$, found in zwitterionic amino acids using a combination of high-resolution (synchroton-source) X-ray crystallography and quantum chemistry, and it has been found that the $\Phi(\mathbf{r})$ values determined computationally were in very good accord with those deduced from the experimental diffraction results.[34−36] We therefore investigated the electrostatic potentials, $\Phi(\mathbf{r})$, for **1**, **2**, **11**, **12**, **19**, and the conjugate base of **19**, using the ionic forms utilized in the CoMFA investigations.

We show in Figure 8A,B the electrostatic potential surfaces $\Phi(\mathbf{r})$ for **1** and **2** projected onto a charge density isosurface, $\rho(\mathbf{r})$, from which it can be seen that most of the charge density in the aromatic ring is located on the H^N pyridinium protons and the immediately adjacent protons. Although the crystallographic structures of **1** and **2** have not yet been determined, the structures of **11** and **12** have been determined,[28,37] and in all three isomers of risedronate determined, as well as in isozo-

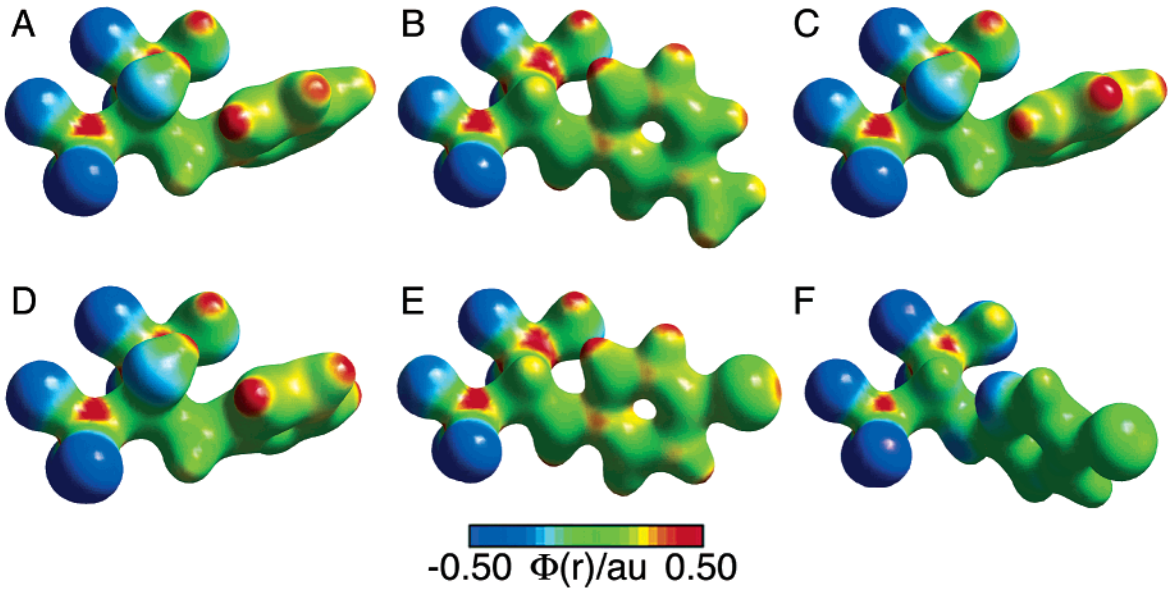

Figure 8. HF/6-311++G(d,p) calculations of the molecular electrostatic potential $\Phi(\mathbf{r})$ mapped onto 0.05 e/a_0^3 charge density $\rho(\mathbf{r})$ isosurfaces for selected bisphosphonates: (A) **1**; (B) **2**; (C) **11**; (D) **12**; (E) **19**; (F) the conjugate base of **19**. Red indicates a positive charge; blue indicates a negative charge region.

ledronate (**12**), the ring nitrogens are protonated, so it seems likely that they will also be protonated in the FPPS active site, forming a (putative) reactive intermediate analogue. With risedronate, as well as isozoledronate, charge appears to be localized primarily on the H^N sites, Figure 8C,D. With the bromopyridine **19**, charge is again clearly located on the H^N atom and the adjacent proton. However, some caution needs to be exercised here because the presence of the halogen can be expected to substantially modify the pK_a of the ring nitrogen. For example, the pK_a values of the *para*- and *meta*-methylpyridines (the parent compounds of **2** and **3**) are 6.06 and 5.71 (to be compared with a pK_a of 5.23 for pyridine, ref 38), while the pK_a values of *ortho*-chloro- and *ortho*-bromopyridine are both 2.84 (39). The possibility exists, therefore, that the ~40−50 μM IC_{50} values for **19** and **22** may in fact be due to substantially lower pK_a values. So, for example, at a nominal pH of 6, **1**−**3** might all reasonably be expected to be ~50% protonated, while **19** and **22** might reasonably be expected to be deprotonated on the ring nitrogens and would not, therefore, be carbocation reactive intermediate analogue inhibitors. A purely steric or repulsive effect in **19** and **22** seems less likely because both **2** and **3** have methyl substitutions, and indeed, in general, the presence of a ring halogen would increase the hydrophobic stabilization of these compounds. Thus, on the basis of these pK_a results, the lack of activity of **19** and **22** may be attributable, at least in part, to an electronic effect of the halogen, in decreasing the pK_a of the pyridinium moiety. As expected, the $\Phi(\mathbf{r})$ for the free base of **19** shows essentially no charge density on any of the ring protons, Figure 8F. On the basis of this possibility, we recomputed the 3D-QSAR/CoMFA equations, excluding **19** and **22** from the training set, thereby predicting the activities of both the protonated and deprotonated species. We found that the pIC_{50} values for the deprotonated forms of **19** and **22** were ~4.5, in very close accord with the experimental ~4.4 and 4.3 values (Table 2), while the pIC_{50} values of the protonated forms were both ~3.8, in worse accord with experiment. However, both protonated and deprotonated species are predicted to be poor growth inhibitors, as found experimentally.

Toxicity of Bisphosphonates. To have any utility as antiparasitic agents, low toxicity is required. To investigate this topic, we next determined the effects of all bisphosphonates on growth of a KB cell line, which is a measure of general cytotoxicity to mammalian cells. We obtained dose-response results for the inhibition of KB cell growth for each of the bisphosphonates investigated, using the Alamar blue technique[40] to obtain LD_{50} values (the dose of bisphosphonate that was lethal to 50% of the KB cells). These LD_{50} values are given in Table 3. When plotted against the IC_{50} values for *T. b. rhodesiense*, Figure 9A, we found essentially no correlation between the LD_{50} results (KB cell cytotoxicity) and the IC_{50} values for *T. b. rhodesiense* replication. Next, to further investigate the relationship between toxicity and antiparasitic activity, we computed therapeutic indices for each of the bisphosphonates investigated, using the following definition:

$$\mathrm{TI} = \frac{\mathrm{LD}_{50}}{\mathrm{IC}_{50}}$$

in which TI is the therapeutic index, LD_{50} is the KB cell LD_{50} and IC_{50} is the IC_{50} for *T. b. rhodesiense* growth inhibition. The results for each compound are given in Table 3. We then plotted these therapeutic index values versus the IC_{50} values for *T. b. rhodesiense* growth inhibition, obtaining the results shown in Figure 9B. Here, the solid circles indicate data points for which discrete LD_{50} values were obtained (14 compounds), while the open circles indicate only lower limits for the therapeutic index (12 compounds) because no toxicity was observed at the highest bisphosphonate levels tested (300 μg/mL). The open square indicates the upper limit of the TI of pamidronate.

This representation should be useful for probing which compounds should be investigated further in animal testing. Specifically, compounds **2**, **3**, **5**, **7**, and

Table 3. IC_{50}, LD_{50}, and Therapeutic Index Results

compound	IC_{50} (μM)[a]	LD_{50} (μM)[b]	TI[c]
1 (*ortho*-risedronate)	0.22	13.9	63
2	0.61	127	208
3	0.70	187	267
4 (ibandronate)	1.0	10.1	10
5 (homorisedronate)	1.7	>804	>473
6	1.7	66.8	39
7	2.0	492	246
8 (olpadronate)	5.4	>1052	>195
9	7.8	977	125
10	8.0	>806	>101
11 (risedronate)	8.6	249	29
12	8.6	41	5
13	19.8	>746	>38
14	20.5	>775	>38
15	20.9	271	13
16	21.3	>931	>44
17 (neridronate)	31.7	680	21
18	34.4	809	24
19	39.5	87	2
20	40.0	218	5
21	50.6	>1149	>23
22	53.3	>992	>19
23	62.4	>993	>16
24	92.0	>967	>11
25	99.8	>1041	>10
26	102	>1149	>11
27 (pamidronate)	≫100	156	<2

[a] IC_{50} values (μM) for *T. b. rhodesiense* trypomastigote growth. From ref 12 and this work (**4**, **6**, **14**, **15**, **18**, **19**, **21**, **22**, **26**). [b] LD_{50} for KB cell growth. The > signs indicate no inhibition found at the highest bisphosphonate level used in the assay, 300 μg/mL. [c] TI = therapeutic index = LD_{50} (KB cells)/IC_{50} (*T. b. rhodesiense*).

8 have TI values of ≳200:1 and relatively low IC_{50} values. The drug olpadronate, **8**, has a TI of ∼200:1 and, as a bisphosphonate in clinical use, appears worthy of further investigation in animal models. Compound **3** is a herbicide[16] also known to have activity in bone resorption,[41] and compound **2** is its isomer. Both have TIs of >200:1 and ∼600−700 nM IC_{50} values for *T. b. rhodesiense* replication. These are all promising indications that at least a subset of the nitrogen-containing bisphosphonates may possess significant antiparasitic activity with low cytotoxicity to mammalian cells.

Conclusions

The results we have reported above are of interest for a number of reasons. First, we provide the first evidence that the enzyme farnesyl pyrophosphate synthase is a principal site of action of the bisphosphonate risedronate in inhibiting the growth of bloodstream-form *T. b. rhodesiense* trypomastigotes, the causative agent of human East African trypanosomiasis. Second, we report a 3D-QSAR/CoMFA analysis of 26 bisphosphonates, yielding a theoretical-versus-experimental pIC_{50} correlation of $R^2 = 0.87$. This is the first report of a QSAR/CoMFA correlation for 1,1-bisphosphonates acting as antiparasitic agents. The predictive capability of this methodology was tested with activity predictions for a series of test compounds. The average pIC_{50} error was 0.23, corresponding to about a factor of 2 error in activity prediction, even though this analysis was performed using data obtained from parasite growth inhibition data, not on a pure enzyme. This is consistent with previous work on *D. discoideum* growth inhibition by bisphosphonates and on bone resorption,[32] suggesting that this approach may have utility in developing

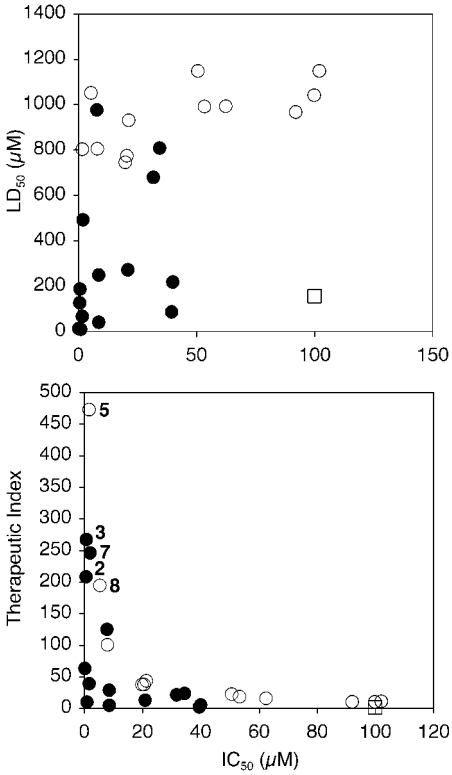

Figure 9. Toxicity/activity data for the bisphosphonates: (A) scatter plot showing LD_{50} (KB cell growth inhibition) versus IC_{50} (*T. b. rhodesiense*) growth inhibition; (B) graph showing the therapeutic index TI = LD_{50}/IC_{50} versus IC_{50} for *T. b. rhodesiense* growth. Compounds **2**, **3**, **5**, **7**, and **8** have high therapeutic indices combined with low IC_{50} values. The solid circles (●) indicate data points for which discrete LD_{50} values were found; the open circles (○) indicate only lower limits to the TI; the open square (□) (**27**) indicates the upper limit to the TI.

novel chemotherapeutic agents on the basis of cell growth rather than just enzyme inhibition data. Third, the results for the aliphatic bisphosphonates show that IC_{50} values decrease rapidly with increasing chain length, at least up to the longest species investigated (**7**, an n-C_{11} side-chain, $IC_{50} = 2.0$ μM). This suggests that even longer chain compounds may have enhanced activity. Moreover, these compounds are known to inhibit FPP synthase from another trypanosomatid, *L. major*. Fourth, we show that the presence of a γ-nitrogen is a necessary but not a sufficient requirement for high activity: only species having γ-nitrogens in an aromatic ring have IC_{50} values <1 μM, presumably a result of charge delocalization and enhanced hydrophobicity. Fifth, our results suggest that ring orientation may also be important: the three most active compounds have different ring geometries, suggesting the more flexible geometry of **1** contributes to its low activity. Sixth, the results of quantum chemical calcuclations show that most charge density in the aromatic rings is located on the H^N and immediately adjacent protons. Seventh, we have investigated the toxicity of these bisphosphonates against mammalian cell growth, identifying a number of compounds that have high activity against *T. b. rhodesiense* proliferation, combined with low toxicity against KB cells. Taken together, these results should be of use in the design and further development of bisphosphonates as antiparasitic agents.

Experimental Section

Drugs. The bisphosphonates not previously investigated as inhibitors of bloodstream-form *T. b. rhodesiense* trypomastigote growth were synthesized and characterized basically according to the methods described in refs 12, 42, and 43. In short, 1-hydroxyalkylidene-1,1-bisphosphonates were prepared by reaction of a carboxylic acid with phosphorous acid and phosphorus trichloride, followed by hydrolysis and pH adjustment to 4.3 with a 50% NaOH solution, followed by recrystallization from H_2O:[12,42]

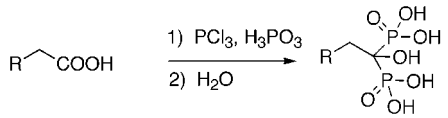

The aminomethylene bisphosphonates were also synthesized basically as described before[12] by reacting stoichiometric amounts of the corresponding amines, triethyl orthoformate, and diethyl phosphite[12,43] followed by acid hydrolysis:

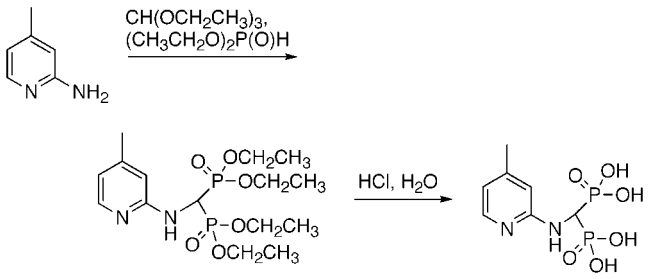

The purity of all new samples was verified by microchemical analysis (H/C/N) and in some cases via ^{13}C, ^{31}P, and ^{1}H NMR spectroscopy. See Supporting Information for analytical data for the target compounds.

Crystallographic Aspects. Single-crystal data for **5** (crystallized from H_2O as the monosodium tetrahydrate salt at pH = 4.6) were collected on a Siemens (Madison, WI) SMART/CCD diffractometer using the SHELXTL V5.0 (Siemens) system and refined by full-matrix least squares on F^2 using all reflections. Hydrogen atoms were assigned idealized locations and given isotropic thermal parameters 1.2 times the thermal parameter of the atom to which they were attached. The data were corrected for Lorentz and polarization effects, and an empirical absorption correction was applied. The crystallographic system, space group, and other information related to the crystal structure determination are summarized in the Supporting Information. Atomic coordinates, bond lengths, angles, and thermal parameters have also been deposited with the Cambridge Crystallographic Data Centre (CCDC). Any request to the CCDC for this material should quote the full literature citation and the reference number.

Data Set and Biological Activity. The in vitro growth inhibition data of bloodstream-form *T. brucei rhodesiense* trypomastigotes (strain STIB 900) by the 17 bisphosphonate compounds investigated previously were from Martin et al.[12] The in vitro growth inhibition data of *T. brucei* trypomastigotes by the additional bisphosphonate compounds were obtained using the same methods. Growth inhibition results are expressed as IC_{50} values, which represent the drug concentrations required to reduce parasite proliferation by 50%.

Growth Inhibition Rescue Studies. Three-fold serial dilutions of **11**, made up in HMI-18 medium supplemented with 20% HIFCS, beginning at an initial concentration of 83.5 μM, were performed in triplicate in 96-well flat-bottom Microtest III tissue culture plates (Becton Dickinson and Company, NJ). This process was repeated for each of the prenyl compounds studied. The compounds geranyl pyrophosphate (GPP), farnesyl pyrophosphate (FPP), and farnesol were added to their respective wells at a final concentration of 12.5 μg/mL. *Trypanosoma brucei rhodesiense* (strain STIB900) bloodstream-form trypomastigotes were then plated in each well at a concentration of 1×10^5/mL. The plates were incubated at 37 °C in a 5% CO_2−air mixture for 72 h followed by the addition of 10 μL/well of Alamar Blue.[40] Plates were incubated for an additional 4 h and read on a Molecular Devices Gemini spectrophotometer at EM/EX 530/585 nm with a cutoff filter at 550 nm. Results were analyzed and IC_{50} values were calculated using Microsoft XLFit (DB Solutions).

3D-QSAR/CoMFA. CoMFA was performed within the QSAR module of Cerius^2 4.6 using default settings. Molecular mechanics calculations were performed with the standard Universal 1.02 force field, with a convergence criterion requiring a minimum energy change of 0.001 kcal/mol. Structures were optimized to convergence at each of the minimization steps. Charge calculations for CoMFA analyses were performed on the minimized structures using the Gasteiger/Hückel method.[44] The CoMFA probe interaction energies were calculated on a rectangular grid around the surface of the aligned molecules. The atomic coordinates of the models were used to compute field values at each point of a 3D grid with a grid spacing of 2.00 Å. CoMFA evaluated the energy between a probe (H^+, CH_3, and donor/acceptor) and a molecule at a series of points defined by the rectangular grid. The 10% of the MFA gridpoints with the highest variance in energy served as input for the calculation of the QSAR. To obtain a quantitative analysis of the dependence of biological activity on MFA parameters, GFA analysis was applied, leading to eq 1.

Quantum Chemical Calculations. Ab initio quantum chemical calculations of the electrostatic potential surfaces ($\Phi(\mathbf{r})$) and charge density isosurfaces ($\rho(\mathbf{r})$) were obtained by using the Gaussian 98W program.[45] We used the Hartree−Fock method with uniform 6-311++G(d,p) basis sets. Bisphosphonate structures used were the molecular mechanics structures shown in Figure 3, with protonated nitrogens and singly deprotonated phosphonate $[P(O)_2(OH)]^{-1}$ groups. The conjugate base of **19** was prepared from **19** and minimized by the same procedure used herein.

Graphics. We used the VMD program[46] to position the alignment of the bisphosphonates in the active site of FPPS (PDB accession number 1UBW), as shown in Figure 4B. VMD was developed by the Theoretical Biophysics Group in the Beckman Institute for Advanced Science and Technology at the University of Illinois at Urbana-Champaign.

Acknowledgment. This work was supported in part by the United States Public Health Service (National Institutes of Health Grant GM-50694 to E. O.) and by the National Computational Science Alliance (Grant MCB000020). M.B.M. is an American Heart Association Predoctoral Fellow, Midwest Affiliate. E.O., H.K., K.deL.-F., and S.L.C. received financial support from the UNDP/World Bank/WHO Special Program for Research and Training in Tropical Diseases (T.D.R.). We thank Scott Wilson for determining the crystallographic structure of **5**.

Supporting Information Available: Tables containing analytical and structural data for the target compounds. This material is available free of charge via the Internet at http://pubs.acs.org.

References

(1) Barrett, M. P. The fall and rise of sleeping sickness. *Lancet* **1999**, *353*, 1113−1114.
(2) Travis, A. S. Paul Ehrlich; a hundred years of chemotherapy 1891−1991. *Biochemist* **1991**, *13*, 9−12.
(3) Dumas, M.; Bouteille, B. Treatment of human African trypanosomiasis. *Bull. W. H. O.* **2000**, *78*, 1474.
(4) Dumas, M.; Bouteille, B. Human African trypanosomiasis. *C. R. Seances Soc. Biol. Ses Fil.* **1996**, *190*, 395−408.
(5) de Koning, H. P.; MacLeod, A.; Barrett, M. P.; Cover, B.; Jarvis, S. M. Further evidence for a link between melarsoprol resistance and P2 transporter function in African trypanosomes. *Mol. Biochem. Parasitol.* **2000**, *106*, 181−185.
(6) McCann, P. P.; Pegg, A. E. Ornthine decarboxylase as an enzyme target for therapy. *Pharmacol. Ther.* **1992**, *54*, 195−215.

(7) Eibl, H.; Unger, C. Hexadecylphosphocholine: a new and selective antitumor drug. *Cancer Treat. Rev*. **1990**, *17*, 233−242.
(8) Jha, T. K.; Sundar, S.; Thakur, C. P.; Bachmann. P.; Karbwang, J.; Fischer, C.; Voss, A.; Berman, J. Miltefosine, an oral agent, for the treatment of Indian visceral leishmaniasis. *N. Engl. J. Med*. **1999**, *341*, 1795−1800.
(9) Rodan, G. A.; Martin, T. J. Therapeutic approaches to bone diseases. *Science* **2000**, *289*, 1508−1514.
(10) Bruchhaus, I.; Jacobs, T.; Denart, M.; Tannich E. Pyrophosphate-dependent phosphofructokinase of *Entamoeba histolytica*: molecular cloning, recombinant expression and inhibition by pyrophosphate analogues. *Biochem. J*. **1996**, *316*, 57−63.
(11) Urbina, J. A.; Moreno, B.; Vierkotter, S.; Oldfield, E.; Payares, G.; Sanoja, C.; Bailey, B. N.; Yan, W.; Scott, D. A.; Moreno, S. N.; Docampo, R. *Trypanosoma cruzi* contains major pyrophosphate stores, and its growth *in vitro* and *in vivo* is blocked by pyrophosphate analogues. *J. Biol. Chem*. **1999**, *274*, 33609−33615.
(12) Martin, M. B.; Grimley, J. S.; Lewis, J. C.; Heath, H. T.; Bailey, B. N.; Kendrick, H.; Yardley, V.; Caldera, A.; Lira, R.; Urbina, J. A.; Moreno, S. N. J.; Docampo, R.; Croft, S. L.; Oldfield, E. Bisphosphonates inhibit the growth of *Trypanosoma brucei*, *Trypanosoma cruzi*, *Leishmania donovani*, *Toxoplasma gondii*, and *Plasmodium falciparum*: A potential route to chemotherapy. *J. Med. Chem*. **2001**, *44*, 909−916.
(13) Moreno, B.; Bailey, B. N.; Luo, S.; Martin, M. B.; Kulhenschmidt, M.; Moreno, S. N. J.; Docampo, R.; Oldfield, E. ^{31}P NMR of Apicomplexans and the effects of risedronate on *Cryptosporidium parvum* growth. *Biochem. Biophys. Res. Commun*. **2001**, *284*, 632−637.
(14) Yardley, V.; Khan, A. A.; Martin, M. B.; Slifer, T. R.; Araujo, F. G.; Moreno, S. N.; Docampo, R.; Croft, S. L.; Oldfield, E. In vivo activities of farnesyl pyrophosphate synthase inhibitors against *Leishmania donovani* and *Toxoplasma gondii*. *Antimicrob. Agents Chemother*. **2002**, *46*, 929−931.
(15) Rodriguez, N.; Bailey, B. N.; Martin, M. B.; Oldfield, E.; Urbina, J. A..; Docampo, R. Cure of experimental cutaneous leishmaniasis using pamidronate. *J. Infect. Dis.*, in press.
(16) Cromartie, T. H.; Fisher, K. J.; Grossman, J. N. The discovery of a novel site of action for herbicidal bisphosphonates. *Pestic. Biochem. Physiol*. **1999**, *63*, 114−126.
(17) van Beek, E.; Pieterman, E.; Cohen, L.; Lowik, C.; Papapoulos, S. Farnesyl pyrophosphate synthase is the molecular target of nitrogen-containing bisphosphonates. *Biochem. Biophys. Res. Commun*. **1999**, *264*, 108−111.
(18) Keller, R. K.; Fliesler, S. J. Mechanism of aminobisphosphonate action: characterization of alendronate inhibition of the isoprenoid pathway. *Biochem. Biophys. Res. Commun*. **1999**, *266*, 560−563.
(19) Bergstrom, J. D.; Bostedor, R. G.; Masarachia, P. J.; Reszka, A. A.; Rodan, G. Alendronate is a specific, nanomolar inhibitor of farnesyl diphosphate synthase. *Arch. Biochem. Biophys*. **2000**, *373*, 231−241.
(20) Dunford, J. E.; Thompson, K.; Coxon, F. P.; Luckman, S. P.; Hahn, F. M.; Poulter, C. D.; Ebetino, F. H.; Rogers, M. J. Structure−activity relationships for inhibition of farnesyl diphosphate synthase in vitro and inhibition of bone resorption in vivo by nitrogen-containing bisphosphonates. *J. Pharmacol. Exp. Ther*. **2001**, *296*, 235−242.
(21) Grove, J. E.; Brown, R. J.; Watts, D. J. The intracellular target for the antiresorptive aminobisphosphonate drugs in *Dictyostelium discoideum* is the enzyme farnesyl diphosphate synthase. *J. Bone Miner. Res*. **2000**, *15*, 971−981.
(22) Eubank, W. B.; Reeves, R. E. Analogue inhibitors for the pyrophosphate-dependent phosphofructokinase of *Entamoeba histolytica* and their effect on culture growth. *J. Parasitol*. **1982**, *68*, 599−602.
(23) Rogers, M. J.; Xiong, X.; Brown, R. J.; Watts, D. J.; Russell, R. G.; Bayless, A. V.; Ebetino, F. H. Structure−activity relationships of new heterocycle-containing bisphosphonates as inhibitors of bone resorption and as inhibitors of growth of *Dictyostelium discoideum* amoebae. *Mol. Pharmacol*. **1995**, *47*, 398−402.
(24) Martin, M. B.; Arnold, W.; Heath, H. T.; Urbina, J. A.; Oldfield, E. Nitrogen-containing bisphosphonates as carbocation transition state analogues for isoprenoid biosynthesis. *Biochem. Biophys. Res. Commun*. **1999**, *263*, 754−758.
(25) Benford, H. L.; Frith, J. C.; Auriola, S.; Monkkonen, J.; Rogers, M. J. Farnesol and geranylgeraniol prevent activation of caspases by aminobisphosphonates: biochemical evidence for two distinct pharmacological classes of bisphosphonate drugs. *Mol. Pharmacol*. **1999**, *56*, 131−140.
(26) Montalvetti, A.; Bailey, B. N.; Martin, M. B.; Severin, G. W.; Oldfield, E.; Docampo, R. Bisphosphonates are potent inhibitors of *Trypanosoma cruzi* farnesyl pyrophosphate synthase. *J. Biol. Chem*. **2001**, *276*, 33930−33937.
(27) *Cerius^2 Modeling Environment*, version 4.6; Accelrys Inc.: San Diego, CA, 2001.
(28) Gossman, W. L.; Wilson, S. R.; Oldfield, E. Three hydrates of 1-hydroxy-2-(3-pyridinyl)ethylidene-1,1-bisphosphonate (Risedronate). *Acta Crystallogr., Sect. C*, submitted for publication.
(29) Van Brussel, E. M.; Gossman, W. L.; Oldfield, E. (Cycloheptylamino)methylene-1,1-bisphosphonate monohydrate (incadronate monohydrate). *Acta Crystallogr., Sect. C*, submitted for publication.
(30) Hasegawa, K.; Funatsu, K. Partial least squares modeling and genetic algorithm optimization in quantitative structure−activity relationships. *SAR QSAR Environ. Res*. **2000**, *11*, 189−209.
(31) Cramer, R. D.; Bunce, J. D.; Patterson, D. E.; Frank, I. E. Crossvalidation, bootstrapping, and partial least squares compared with multiple regression in conventional QSAR studies. *Quant. Struct.−Act. Relat*. **1988**, *7*, 18−25.
(32) Szabo, C. M.; Martin, M. B.; Oldfield, E. An investigation of bone resorption and *Dictyostelium discoideum* growth inhibition by bisphosphonate drugs. *J. Med. Chem.*, in press.
(33) Szabo, C. M.; Matusmura, Y.; Fukura, S.; Martin, M. B.; Sanders, J. M.; Sengupta, R.; Cieslak, J.; Loftus, T. C.; Lea, C. R.; Lee, H.-J.; Koohang, A.; Coates, R.; Sagami, H.; Oldfield, E. Inhibition of Geranylgeranyl Diphosphate Synthase by Bisphosphonates and Diphosphates: A Potential Route to New Bone Antiresorption and Antiparasitic Agents. *J. Med. Chem*. **2002**, *45*, 2185−2196.
(34) Arnold, W. D.; Sanders, L. K.; McMahon, M. T.; Volkov, A. V.; Wu, G.; Coppens, P.; Wilson, S. R.; Godbout, N.; Oldfield, E. Experimental, Hartree−Fock, and density functional theory investigations of the charge density, dipole moment, electrostatic potential, and electric field gradients in L-asparagine monohydrate. *J. Am. Chem. Soc*. **2000**, *122*, 4708−4717.
(35) Destro, R.; Roversi, P.; Barzaghi, M.; Marsh R. E. Experimental charge density of glycine at 23 K, *J. Phys. Chem. A* **2000**, *104*, 1047−1054.
(36) Flaig, R.; Koritsanszky, T.; Zobel, D.; Luger, P. Topological analysis of the experimental electron densities of amino acids. 1. D,L-aspartic acid at 20 K. *J. Am. Chem. Soc*. **1998**, *120*, 2227−2238.
(37) Gossman, W. L.; Oldfield, E. Monosodium 1-hydroxy-2-(1, 3*H*-imidazol-4-yl)ethylidene-1,1-bisphosphonate tetrahydrate (isozoledronate monosodium). *Acta Crystallogr., Sect. C*, submitted for publication.
(38) Hallé, J.-C.; Lelievre, J; Terrier, F. Solvent effect on preferred protonation sites in nicotinate and isonicotinate anions. *Can. J. Chem*. **1996**, *74*, 613−620.
(39) *CRC Handbook of Chemistry and Physics*, 70th ed.; Weast, R. T., Ed.; CRC Press Inc.: Boca Raton, FL, 1989; p D-162.
(40) Raz, B.; Iten, M.; Grether-Buhler, Y.; Kaminsky, R.; Brun, R. The Alamar Blue assay to determine drug sensitivity of African trypanosomes (*T. b. rhodesiense* and *T. b. gambiense*) in vitro. *Acta Trop*. **1997**, *68*, 139−147.
(41) Sunberg, R. J.; Ebetino, F. H.; Mosher, C. T.; Roof, C. F. Designing drugs for stronger bones. *Chemtech* **1991**, *21*, 304−309.
(42) Kieczykowski, G. R.; Jobson, R. B.; Melillo, D. G.; Reinhold, D. F.; Grenda, V. J.; Shinkai, I. Preparation of (4-amino-1-hydroxybutylidene) bisphosphonic acid sodium salt, MK-217 (alendronate sodium). An improved procedure for the preparation of 1-hydroxy-1,1-bisphosphonic acids. *J. Org. Chem*. **1995**, *60*, 8310−8312.
(43) Soloducho, J.; Gancarz, R.; Wieczorek, P.; Korf, J.; Hafner, J.; Lejczak, B.; Kafarski, P. Patent PL93−298436 93408, 1993.
(44) Gasteiger, J.; Marsili, M. Iterative partial equalization of orbital electronegativity: a rapid access to atomic charges. *Tetrahedron* **1980**, *36*, 3219−3222.
(45) Frisch, M. J.; Trucks, G. W.; Schlegel, H. B.; Scuseria, G. E.; Robb, M. A.; Cheeseman, J. R.; Zakrzewski, V. G.; Montgomery, J. A., Jr.; Stratmann, R. E.; Burant, J. C.; Dapprich, S.; Millam, J. M.; Daniels, A. D.; Kudin, K. N.; Strain, M. C.; Farkas, O.; Tomasi, J.; Barone, V.; Cossi, M.; Cammi, R.; Mennucci, B.; Pomelli, C.; Adamo, C.; Clifford, S.; Ochterski, J.; Petersson, G. A.; Ayala, P. Y.; Cui, Q.; Morokuma, K.; Malick, D. K.; Rabuck, A. D.; Raghavachari, K.; Foresman, J. B.; Cioslowski, J.; Ortiz, J. V.; Stefanov, B. B.; Liu, G.; Liashenko, A.; Piskorz, P.; Komaromi, I.; Gomperts, R.; Martin, R. L.; Fox, D. J.; Keith, T.; Al-Laham, M. A.; Peng, C. Y.; Nanayakkara, A.; Gonzalez, C.; Challacombe, M.; Gill, P. M. W.; Johnson, B. G.; Chen, W.; Wong, M. W.; Andres, J. L.; Head-Gordon, M.; Replogle, E. S.; Pople, J. A. *Gaussian 98*, revision A.7; Gaussian, Inc.: Pittsburgh, PA, 1998.
(46) Humphrey, W.; Dalke, A.; Schulten, K. VMD−Visual Molecular Dynamics. *J. Mol. Graphics*, **1996**, *14*, 33−38.

JM0102809